ChemComm

Accepted Manuscript

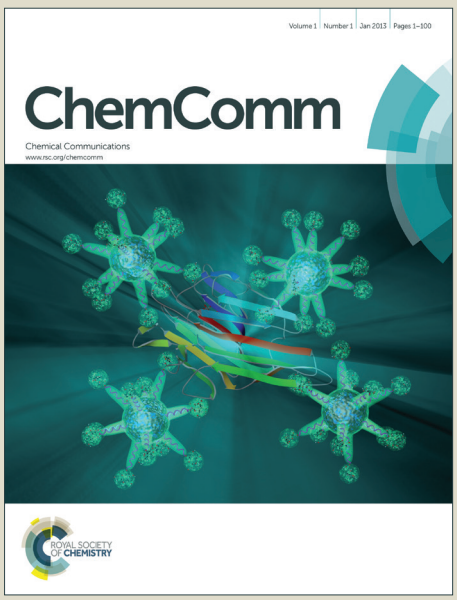

ROYAL SOCIETY OF CHEMISTRY

www.rsc.org/chemcomm

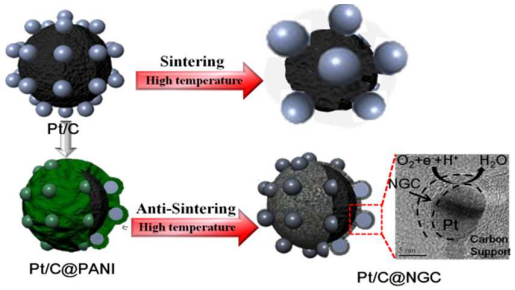

The nitrogen-doped graphitic carbon layer was elaborately introduced to the Pt/C surface and Pt NPs can survive from the pyrolyzation.

Journal Name

RSCPublishing

COMMUNICATION

Pt/C Trapped in Activated Graphitic Carbon Layers as a Highly Durable Electrocatalyst for Oxygen Reduction Reaction

Cite this: DOI: 10.1039/x0xx00000x

Received 00th January 2012,
Accepted 00th January 2012

DOI: 10.1039/x0xx00000x

www.rsc.org/

Yao Nie, Siguo Chen,* Wei Ding, Xiaohong Xie, Yun Zhang and Zidong Wei*

A thin nitrogen-doped graphitic carbon layer is elaborately introduced to the Pt/C surface to not only inhibit migration and dissolution of Pt nanoparticles, but also impart activity to the integral catalyst without blocking the inner Pt catalytic active sites. Corrosion of carbon support also can be alleviated due to the outer graphitic coverage.

Proton exchange membrane fuel cells (PEMFCs) have drawn significant attention as a novel alternative to traditional power sources due to their high energy conversion efficiency and low environmental impact.[1] However, the sluggish kinetics of oxygen reduction reaction (ORR) on the cathode, on the one hand, demand high loading of active Pt-based catalysts, which unfavorably increases the cost of PEMFCs systems. [2] Considerable efforts have been dedicated to reducing Pt consumption by alloying Pt with transition metals as well as by exploring nonprecious metal catalyst concepts. [3]On the other hand, the poor long-term stability of standard and advanced ORR electrocatalysts is remaining a major obstacle. [4] To address the question of stability in a rational manner, the degradation mechanisms of the catalysts in the PEMFCs system need to be understood and considered for the design of new electrocatalyst materials. Degradation of the most commonly used ORR catalysts, Pt nanoparticles (NPs) on carbon supports, predominantly occurs under harsh potential fluctuations, particularly during start-up and shut-down (start-stop) cycles where the electrode potential can locally reach values up to 1.5 V. [5] At these high potentials, Pt dissolution, eventually followed by particle growth due to Ostwald ripening (i.e., dissolution of small Pt particles and redeposition of the Pt species from solution at larger particles), might occur. [6] Pt NPs can also easily migrate on the carbon supports due to the weak interactions with the carbon support and subsequently agglomerate. [7] Furthermore, corrosion of the carbon support accompanied with the detachment of Pt nanoparticles from the support can take place.[8] Extensive research has been conducted to mitigate the above mentioned degradation modes. Decorating Pt NPs surface with molecules and tuning the chemical and physical properties of the carbon supports can suppress the migration and agglomeration of Pt NPs to some extent.[9] However, these methods are not effective for the suppression of the growth of Pt NPs through Ostwald ripening. Although some methods have been developed to covering Pt NPs surface with polymer, carbon or silica layer and have resulted in excellent stabilities, [10] the ORR activity of these catalysts was only slightly improved and no reports have focused on inhibiting agglomeration and dissolution of Pt NPs by covering Pt surface with an active sites-containing layer to realize both superior durability and high activity.

Herein, we designed a novel strategy to address both durability and activity issues via coating a nitrogen-doped graphitic carbon (NGC) layer onto the surface of Pt/C catalyst. The NGC, which is usually employed as an ameliorative carbon support or a promising Pt-free ORR catalyst, [11] is elaborately introduced to the Pt/C surface to not only restrain migration and dissolution of Pt NPs, but also act as the secondary active site supplier that imparting activity to the integral catalyst without blocking the inner Pt catalytic active sites. Serious corrosion of carbon support also can be alleviated due to the protection of the graphitic outer cover. This new nanoarchitecture, incorporating simultaneously above desirable design rationales, exhibits much improved durability and activity over commercial Pt/C for ORR.

The overall synthetic strategy of NGC-trapped Pt/C is illustrated in Figure 1. Polyaniline (PANI) was employed as the NGC precursor and polymerized in situ on the surface of the Pt/C catalyst (denoted as Pt/C@PANI), followed by subjecting Pt/C@PANI to graphitization under an inert atmosphere at 900ºC to yield NGC shell. During the heat-treatment process, the Pt NPs tended to sinter either by coalescence of smaller particles (entire NPs move over the support surface and eventually collide and coalesce with other NPs)

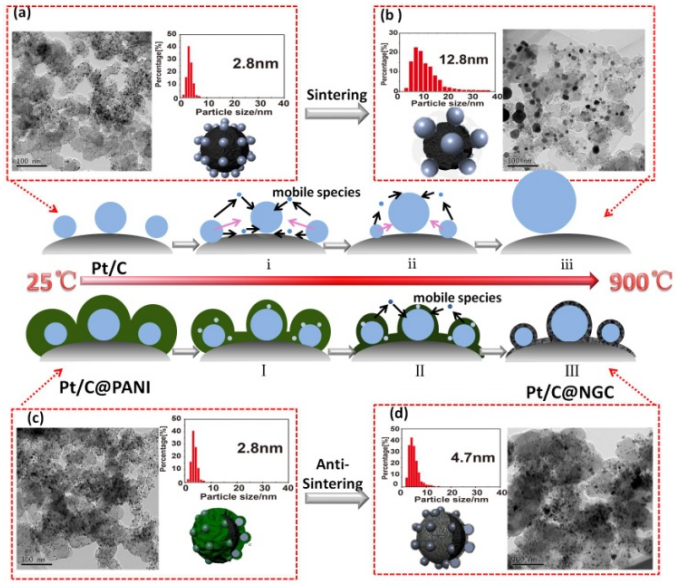

Fig. 1 The synthetic strategy of Pt/C@NGC. TEM and Pt particle-distribution histograms of (a) Pt/C, (b) Pt/C directly subjected to the heat-treatment without PANI protection, (c) Pt/C@PANI, (d)Pt/C@NGC. The scale bar in all TEM images is 100nm. ⅰ - ⅲ represent occurrence of serious Ostwald ripening and interparticle coalescence during the heat-treatment process. Ⅰ -Ⅲ represent the critical role of PANI in stabilizing Pt NPs during the heat-treatment process.

or by Ostwald ripening involving interparticle transport of mobile species (i.e., adatom), with larger particles growing at the expense of smaller particles, as illustrated in (i)-(iii) in Fig.1.[12] The thermally-induced growth of NPs can result in a dramatic drop of activity due to the loss of active surface area, [13] which should be considered and solved in designing and synthesizing advanced catalysts. Fortunately, the NGC precursor, PANI, was ingeniously used to inhibit Pt NPs from serious sintering, thus guaranteeing the feasibility of the design concept of the Pt/C@NGC. At lower temperature, the coverage of PANI network was thick enough to trap Pt NPs and the mobile species detached from smaller particles efficiently. With the temperature increasing, the thickness of PANI became thinner due to the PANI decomposition and the mobility of Pt NPs and mobile species became flexible, as illustrated in (Ⅰ)-(Ⅲ) in Fig.1 (the decomposition temperature was determined by thermal gravimetric analysis as shown in Fig.S1). Despite the inevitable growth of Pt NPs, the critical role of PANI in stabilizing Pt NPs during the heat-treatment process is still highlighted and directly confirmed by the representative transmission electron microscopy (TEM). As shown in Fig.1d, no obvious Pt conglomeration occurs and the average particle size of Pt/C@NGC increases only ~2nm (Fig.1b) when compared with the pristine Pt/C catalyst (Fig.1a). In sharp contrast, the average particle size of the Pt/C catalysts which was directly subjected to the heat-treatment without PANI protection increases from 2~3nm to 12~13 nm and the size distribution of Pt NPs becomes wider (Fig. 1b).

Further morphology observation using high-resolution transmission electron microscopy (HRTEM) images clearly demonstrate the core-shell structure of Pt/C@NGC catalyst before and after heat treatment. The HRTEM in Fig.2c reveals the lattice fringes with a distance of 0.23 nm matching well with d spacing of (111) plane of face-centered cubic (fcc) crystalline Pt, as well as the lattice fringes in outer part with a distance of 0.34 nm, corresponding to the graphitic carbon shell. The HRTEM analysis also discloses that the thickness of decoration layer for Pt/C@PANI and Pt/C@NGC shrinks from 11nm to 3nm, suggesting that the substantial PANI decompose during heat-treatment as mentioned above.[14] An extensive physical characterization was conducted to further reveal the transformation of the decoration layer. The fourier transform infrared (FT-IR) spectra analysis (the inset of Fig.2a) reveal that benzene (1146 cm^{-1}) and quinone-type (1497 cm^{-1}) structures on the main PANI chain are lost after heat treatment, further confirming that PANI decomposed and new active sites were generated. The elemental surface composition information from X-ray photoelectron spectroscopy (XPS) further confirms the formation of NGC shell. Compared with pristine Pt/C catalyst, the XPS survey scan of Pt/C@NGC catalyst reveals the presence nitrogen (Fig.S2). Since the nitrogen doped into the carbon structure is likely to play a role inducing ORR activity of the PANI-derived catalysts, nitrogen functionality in Pt/C@NGC determined by N 1s XPS spectra was studied. As depicted in Fig.2d, the N1s spectra can be deconvoluted into four peaks, which are assigned to N oxide (402.2eV), graphitic N (401.4eV), pyrrolic N (400.1eV) and pyridinic N (398.8eV), with compositions of 10.6, 30.4, 54.8 and 4.1at%, respectively. The binding energy for each type of N was selected according to the previous reports. [15] The deconvolution results clear indicate that the Pt/C@NGC catalyst shows a high ratio of pyrrolic N.

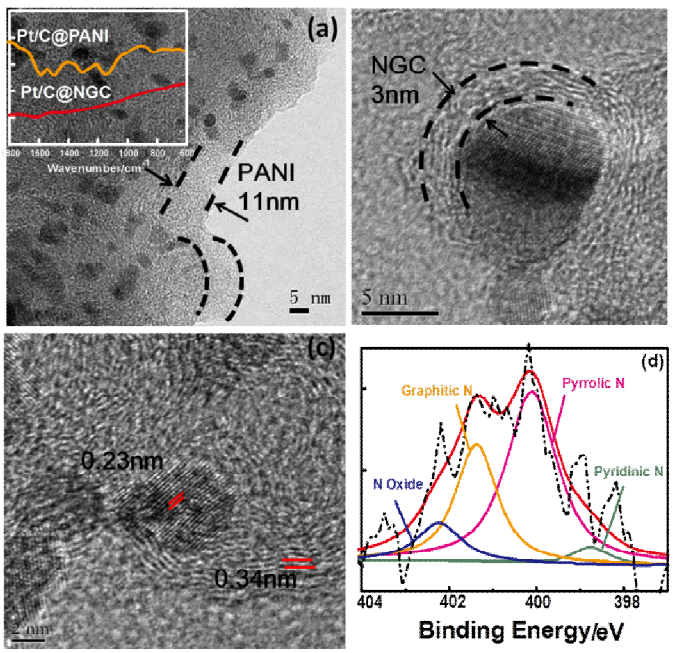

Fig. 2 HRTEM images of (a) Pt/C@PANI, (b) (c) Pt/C@NGC; (d) N 1s XPS spectra of Pt/C@NGC.The inset in (a) shows a FT-IR spectrum for Pt/C@PANI and Pt/C@NGC.

The effect of NGC shell on the electrochemical performance of the Pt/C@NGC catalyst is presented in Fig.3. Fig.3a shows the cyclic voltammetry (CV) curves for the different catalysts, which were recorded in an N_2-saturated 0.1M $HClO_4$ solution at a scan rate of 50mV·s^{-1}. Two peak couples are found in the potential range of 0.05-0.4 V and 0.6-1.2 V in the CV for Pt/C. The former peak couples are assignable to the hydrogen adsorption and desorption on Pt metal, and the latter peaks are due to the oxidation and reduction of Pt. These peak couples due to Pt metal are also observed in the CV for Pt/C@NGC, implying that NGC would not block the transport of aqueous electrolyte to the inner Pt active sites. The electrochemical surface area (ECSA, see in ESI) based on the Pt

mass for Pt/C and Pt/C@NGC are estimated to be 74.7m^2g^{-1} and 46.2m^2g^{-1}, respectively.

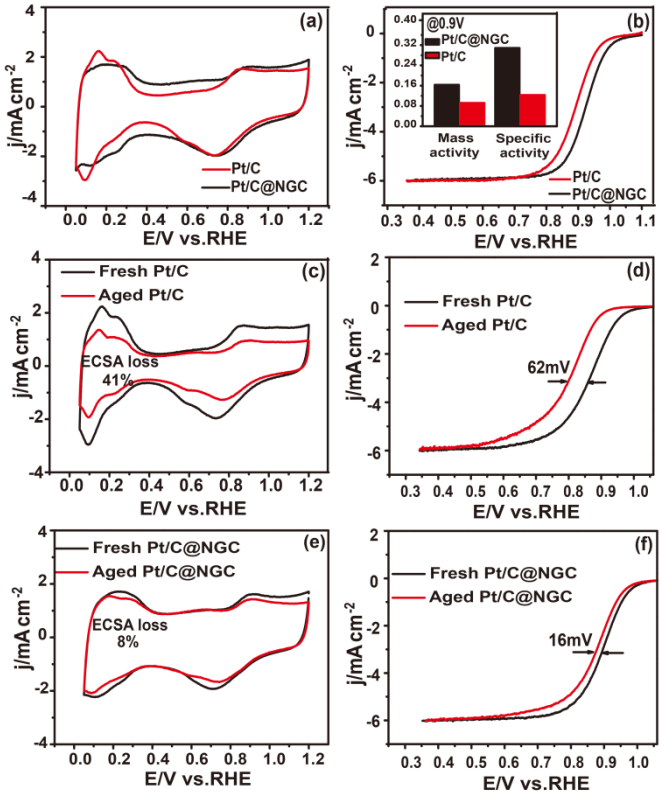

Fig. 3 (a) Cyclic voltammograms for Pt/C and Pt/C@NGC catalysts in N_2-saturated 0.1M $HClO_4$ solution at room temperature with a sweep rate of 50mV/s. (b) Polarization curves for Pt/C and Pt/C@NGC catalysts at a rotating speed of 1600rpm in an O_2-saturated 0.1M $HClO_4$ solution at 60 ºC with a sweep rate of 10mV/s, Pt loading of all electrodes are 51μg/cm^2. The inset in (b) is mass activities and specific activities at 0.9V for Pt/C and Pt/C@NGC catalysts. Cyclic voltammograms for (c) Pt/C and (e) Pt/C@NGC before and after 1500 cycles in N_2-saturated 0.1M $HClO_4$ solution at room temperature with a sweep rate of 50mV/s. Polarization curves for (d) Pt/C and (f) Pt/C@NGC before and after 1500 cycles at a rotating speed of 1600rpm in an O_2-saturated 0.1M $HClO_4$ solution at 60 ºC with a sweep rate of 10mV/s.

ORR measurements were performed in O_2-saturated 0.1 M $HClO_4$ electrolyte using a rotating disk electrode (RDE) at a rotating rate of 1600 rpm. The polarization curves for all catalysts are shown in Figure 3b. It can be seen that the half wave potential for Pt/C@NGC catalyst is 0.923V vs. reversible hydrogen electrode (RHE) which is 32 mV higher than pure Pt/C catalyst, indicating the higher catalytic activity of Pt/C@NGC for ORR. The Tafel plots derived from the mass-transport correction of corresponding RDE data are provided to further evaluate the catalytic kinetics for ORR (Fig.S3b). The Tafel slope of the Pt/C@NGC is calculated as 16 mV per decade, lower than that of Pt/C (27mV per decade), suggesting its favorable reaction kinetics. Furthermore, specific activities of two catalysts are also calculated based on the kinetic current density obtained at 0.9V and 0.95 V. As shown in Fig.3b, the Pt/C@NGC catalyst exhibits a specific activity of 0.308mAcm^{-2} at 0.9 V, which is 2.5 times greater than that of Pt/C (0.123mAcm^{-2}). After normalization to the loading amount of Pt metal, the mass activity of Pt/C@NGC catalyst is found to be 163mAmg$^{-1}_{Pt}$, which is 1.7 times greater than that of Pt/C (92mAmg$^{-1}_{Pt}$). At 0.95V, the specific activity and mass activity for Pt/C@NGC is 0.094mAcm^{-2} and 51.9mAmg$^{-1}_{Pt}$, respectively (Fig.S3a). These values are 3.3 times and 2.5 times higher than those of Pt/C. The carbon supported NGC alone without Pt NPs (denoted as NGC/C) was also prepared and it exhibited certain ORR catalytic activity (Fig.S4). Despite the NGC contributes to supplying activity to the integral catalyst, the reason why Pt/C@NGC exhibits higher activity with larger Pt NPs needs to be explained. According to the observation reported by Arenz and co-workers, size effect on the ORR activity is indistinctively for Pt NPs with a diameter below 5 nm[16] (the NP size in Pt/C@NGC is 4.7nm) and in fact only relatively small differences in specific activity were observed between catalysts with particle sizes ≤5nm.[1, 17] Thus, the much improved ORR catalytic activity can be attributed to the merits of unique designed nanoarchitecture featured with dual active sites.

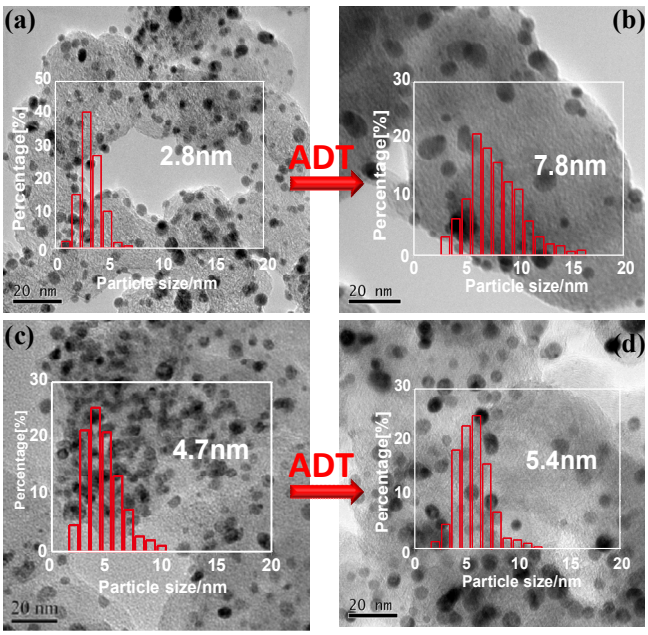

Fig. 4 TEM images of (a) fresh Pt/C catalyst, (b) Pt/C catalyst after 1,500 CV cycles, (c) fresh Pt/C@NGC catalyst, and (d) Pt/C@NGC catalyst after 1,500 CV cycles.

The stability of the Pt/C@NGC catalyst was evaluated through accelerated durability tests (ADT), which were performed at room temperature in N_2-saturated 0.1M $HClO_4$ solution with the application of cyclic potential sweeps between 0.0 and 1.2 V vs.RHE at a scan rate of 50 mV·s^{-1}. After 1500 cycles, the Pt/C@NGC catalyst shows 8% diminution in the Pt ECSA and only a 16mV degradation in half-wave potential (Fig.3e, f), whereas the loss of Pt ECSA is as high as 41% and the shift in the half-wave potential was 61mv for Pt/C catalyst (Fig.3c, d). The morphologies of the NGC-trapped Pt/C catalyst and un-trapped Pt/C catalyst before and after the CV cycling were examined by TEM (Fig.4). After ADT, Pt NPs in un-trapped Pt/C shows serious agglomeration and the number of Pt NPs remarkably decreases in vision due to the dissolution and detachment of Pt NPs. The size of Pt NPs in un-trapped Pt/C increased from 2~3 nm to 10~11 nm with a broad size distribution (Fig.4a, b). In contrast, there is essentially no perceptible change in the integral distribution and the size of the NPs in NGC-trapped Pt/C catalyst (Fig.4c, d). These results highlight the value of the NGC in stabilizing Pt NPs and protecting carbon support.

Conclusions

In summary, we have successfully designed and synthesized a novel Pt/C@NGC catalyst in which the Pt/C catalyst was trapped in nitrogen-doped graphitic carbon layers. The Pt NPs size in Pt/C@NGC catalyst are only 4.7nm even after 900ºC heat treatment, as compared to the 12.8nm for un-trapped Pt/C catalyst heated to the

same temperature, which was attributed to the confinement effect of PANI network. The as-constructed Pt/C@NGC catalyst exhibit evidently enhanced stability and activity toward ORR when compared with the un-trapped Pt/C catalyst, which definitely discloses the merits of elaborately designed nanoarchitecture featured with an integration of Pt/C and NGC. Apart from contributing to active site formation and allowing the reactants to access without blocking the inner Pt catalytically active sites, the NGC sheath can also prevent Pt NPs from aggregation and protect carbon support from directly exposure to the harsh working environment, consequently improving the structural integrity, chemical stability and the corrosion resistance of resulting catalyst in acidic and oxidative environments. The thickness of the NGC, which can be controlled by varying the content of PANI, deserves further study, as the ORR performance may be partly affected by the NGC thickness. The certified perfect construction of carbon-supported Pt core and N-containing graphitic carbon shell may offer a persuasive approach toward advanced functional nanomaterials for fuel cell.

This work was financially supported by the China National 973 program (2012CB720300 and 2012CB215500), the NSFC of China (Grants 21176327, 51272297 and 21276291).

Notes and references

The State Key Laboratory of Power Transmission Equipment & System Security and New Technology, College of Chemistry and Chemical Engineering, Chongqing University, Chongqing,400044 (China)
Fax: +86 23 65102531;
E-mail: zdwei@cqu.edu.cn (Wei);
E-mail: csg810519@126.com (Chen)

† Electronic Supplementary Information (ESI) available: the details of experimental procedures, electrochemical tests, thermal gravimetric analysis, XPS analysis and stability test. See DOI: 10.1039/c000000x/

1 H. A. Gasteiger, S. S. Kocha, B. Sompalli, F. T. Wagner, *Appl. Catal. B* 2005, **56**, 9.
2 J. Tian, A. Morozan, M. T. Sougrati, M. Lefèvre, R. Chenitz, J. P. Dodelet, D. Jones, F. Jaouen, *Angew. Chem.,* 2013, **125**, 7005; *Angew. Chem. Int. Ed.* 2013, **52**, 6867.
3 (a) H. I. Karan, K. Sasaki, R. R. Adzic*, ACS Catal.,* 2012, **2**, 817; (b) S. Yoo, S. Kim, T. Jeon, S. Hwang, J. Lee, S. Lee, K. Lee, Y. Cho, Y. Sung, T. Lim, *Chem. Commun.*, 2011, **47**, 11414; (c) J. X. Wang, H. Inada, L. J. Wu, Y. M. Zhu, Y. M. Choi, P. Liu, W. P. Zhou, R. R. Adzic, *J. Am. Chem. Soc.,* 2009, **131**, 17298; (d) G. Wu, K. L. More, C. M. Johnston, P. Zelenay, *Science,* 2011, **332**, 443.
4 P. J. Ferreira, G. J. la O', Y. S. Horn, D. Morgan, R. Makharia, S. Kocha, H. A. Gasteiger, *J. Electrochem. Soc.,* 2005, 152, A2256.
5 (a) C. Hartnig, T. J. Schmidt, *J. Power Sources,* 2011, **196**, 5564; (b) K. Kinoshita, J. T. Lundquist, P. Stonehart, *J. Electroanal. Chem. nterfacial lectrochem.,* 1973**, 48**, 157; (c) J. C. Meier, C. Galeano, I. Katsounaros, A. A. Topalov, A. Kostka, F. Schüth, K. J. J. Mayrhofer, *ACS Catal.*, 2012, **2**, 832; (d)T. J. Schmidt, J. Baurmeister, *J. Power Sources*, 2008, **176**, 428; (e)H. Tang, Z. Qi, M. Ramani, J. F. Elter, *J. Power Sources,* 2006, **158**, 1306.
6 Y. S. Horn, W. Sheng, S. Chen, P. Ferreira, E. Holby, D. T. Morgan, *Catal.,* 2007, **46**, 285.
7 (a) S. Donthu, M. Cai, M. Ruthkosky, I. Halalay, *Chem. Commun.*, 2009, **4**, 4203; (b) Y. Chung, C. Pak, G. S. Park, W. S. Jeon, J. R. Kim, Y. Lee, H. Chang, D. J. Seung, *J. Phys. Chem. C,* 2008, **112**, 313; (c) G. S. Park, C. Pak, Y. S. Chung, J. R. Kim, W. S. Jeon, Y. H. Lee, K. Kim, H. Chang, D. J. Seung, *J. Power Sources,* 2008, **176**, 48.
8 (a) E. Antolini, E. R. Gonzalez, *Solid State Ionics,* 2009, **180**, 746; (b) L. Castanheira, L. Dubau, M. Mermoux, G. Berthomé, N. Caqué, F. Maillar, *ACS Catal.*, 2014, **4**, 2258; (c) S. Y. Huang, P. Ganesan, S. Park, B. N. Popov, *J. Am. Chem. Soc.* 2009, **131**, 13898; (d) S. E. Jang, H. Kim, *J. Am. Chem. Soc.,* 2010, **132**, 14700.
9 (a) K. Miyabayashi, H. Nishihara, M. Miyake, *Langmuir,* 2014, **30**, 2936; (b) A. C. Ferrandez, S. Baranton, J. Bigarré, P. Buvat, C. Coutanceau, *Chem. Mater.,* 2013, **25**, 3797; (c) Z. Zhou, X. Kang, Y. Song, S. Chen, *Chem. Commun.,* 2010, **48**, 3391; (d) D. Strmcnik, M. E. Escribano, K. Kodama, V. R. Stamenkovic, A. Cuesta, N. M. Markovic, *Nat. Chem.,* 2010, **2**, 880; S. Chen, Z. Wei, L. Guo, W. Ding, L. Dong, P. Shen, *Chem Commun.,* 2011, **47**, 10984.
10 (a) Z. Z. Jiang, Z. B. Wang, D. M. Gu, E. S. Smotkin, *Chem Commun.,* 2010, **46**, 6998; (b) S. Chen, Z. Wei, X. Qi, L. Dong, *J. Am. Chem. Soc.,*2012, **134**, 13252; (c) S. Takenaka, H. Matsumori, K. Nakagawa, Y. Utsunomiya, H. Matsune, M. Kishida, *J. Phys. Chem. C,* 2014, **118**, 774.
11 (a) W. Ding, Z. D. Wei, S. G. Chen, X. Q. Qi, T. Yang, J. S. Hu, D. Wang, L. J. Wan, S. F. Alvi, L. Li, *Angew. Chem. Int. Ed.,* 2013, **52**, 1; (b) C. S. Liu, X. C. Liu, G. C. Wang, R. P. Liang, J. D. Qiu, *Journal of Electroanalytical Chemistry*, 2014, **728**,41; (c) J. Sanetuntikul, T. Hang, S. Shanmugam, *Chem Commun.,* 2014, **50,** 9473; (d) S. Pylypenko, A. Borisevich, K. L. More, A. R. Corpuz , T. Holme, A. A. Dameron, T. S. Ols on, H. N. Dinh, R. O'Hayre, *Energy Environ. Sci.,* 2013, **6**, 2957.
12 (a) T. W. Hansen, A. T. Delariva, S. R. Challa, A. K. Datye, *Accounts of Chemical Research* 2013, **46**, 1720; (b)F. Cosandey, T. E. Madey, *Surf. Rev. Lett.* 2001, **8**, 73.
13 J. M. Thomas, W. J. Thomas, Principles and Practice of Heterogeneous Catalysis, VCH, Weinheim, 1997.
14 J. R. Pels, F. Kapteijn, J. A. Moulijn, Q. Zhu, K. M. Thomas, *Carbon* 1995, **33**, 1641.
15 M. Ferrandon, A. J. Kropf, D. J. Myers, *J. Phys. Chem. C,* 2012, **116**, 16001; (b) H. Jin, H. Zhang, H. Zhong and J. Zhang., *Energy Environ. Sci.,* 2011, **4**, 3389; (c) L. Qie, W. M. Chen, L. X. Yuan, X. L. Hu, W. X. Zhang, Y. H. Huang, *Adv. Mater.*, 2012, **24**, 2047. (d) G. Wu, M. A. Nelson, N. H. Mack, S. G. Ma, P. Sekhar, F. H. Garzon, P. Zelenay, *Chem. Commun.*, 2010, **46**, 7489.
16 M. Nesselberger, S. Ashton, J. C. Meier, M. Arenz, *J. Am. Chem. Soc.,* 2011, **133**, 17428.
17 (a) Y. Takasu, N. Ohashi, X. G. Zhang, Y. Murakami, H. Minagawa, S. Sato, K. Yahikozawa, *Electrochim. Acta,* 1996, **41**, 2595; (b) K. J. J. Mayrhofer, D. Strmcnik, B. B. Blizanac, V. Stamenkovic, M. Arenz, N. M. Markovic, *Electrochim. Acta* 2008, **53**, 3181.

